

# ***GROT* in NICMOS Cameras**

---

M. Sosey, E. Bergeron  
September 20, 1999

---

## **ABSTRACT**

*Grot* is exhibited as small areas of reduced sensitivity, most likely due to flecks of anti-reflective paint scraped off the optical baffles as they were forced against each other. This paper characterizes *grot* associated with all three cameras. Flat field images taken from March 1997 through January 1999 have been investigated for changes in the *grot*, including possible wavelength dependency and throughput characteristics. The main products of this analysis are *grot* masks for each of the cameras which may also contain any new cold or dead pixels not specified in the data quality arrays.

---

## **1. Introduction**

Shortly after launch, orbital testing of NICMOS revealed that expansion of solid nitrogen deformed the dewar leading to thermal contact between the instrument cold well and the inner vapor-cooled shield. Debris on the detector surfaces are believed to be bits of anti-reflective paint scraped off the optical baffles when they were pushed against each other. These paint flecks, now referred to as *grot*, can be found on each of the detectors and are characterized by small areas of reduced sensitivity. The largest example, now known as the “battleship” feature can be seen in camera 1 (see Figure 1) and affects approximately 35 pixels. Scrape tests conducted at Ball Aerospace shortly after NICMOS was launched, using the same type of paint found on the NICMOS baffles, reveal that the paint flecks can range in size from 25 $\mu\text{m}$  to greater than 100 $\mu\text{m}$  (see Figure 3). Since NICMOS pixels are 40 $\mu\text{m}$  on a side, this means there is potential for *grot* smaller than 1 pixel. *Grot* affects approximately 250 pixels in each of the cameras, or less than 1% of the total number of pixels in each detector (See Table 1).

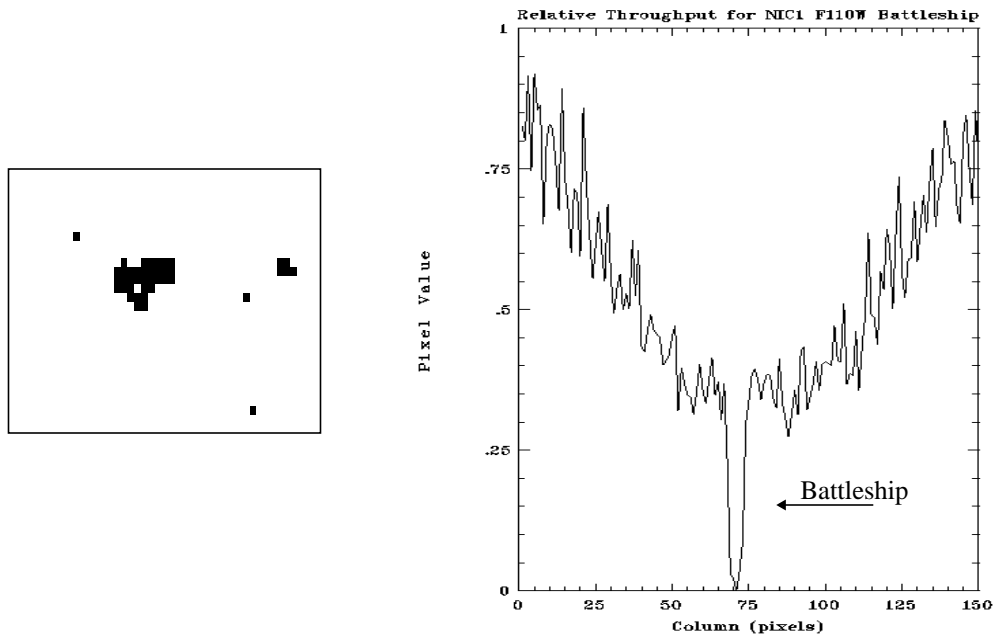


**Figure 1:** The “battleship” feature in camera 1 and its relative throughput. The graph on the right was normalized with a rough estimate of the mean signal from a calibrated image. No “cleaning” was performed before the mean was calculated.

Figure 2 shows a plot made during SMOV activities in 1997 which illustrates the increase in low-transmission pixels. It shows a dramatic increase approximately when the dewar anomaly occurred, as grot began to accumulate on the detectors. It should be noted that it’s not really possible to count the pieces of grot, merely the number of affected pixels.

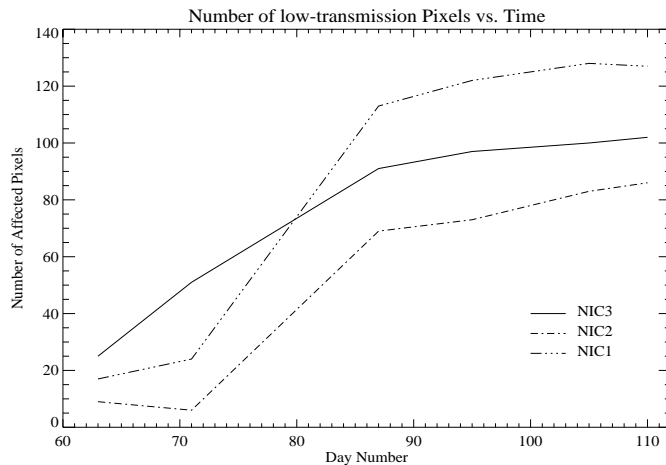


**Figure 2:** Plot from SMOV activities detailing the increase in low-transmission pixels from February 1997 - May 1997 as a result of the dewar anomaly.

## 2. Analysis

All images used in this analysis were flat-fields taken from the programs 7689, 7690, 7814, 7956, 7957, 7961, 8083, 8084. These programs were designed to monitor flat-field stability. Along with the SMOV data from programs 7035, 7134, 7041, 7042, 7150, 7046, 7043, 7608 and 7901, they represent the only chronological breakdown of data to investigate changes in the grot over the initial life of the instrument (February 1997 to January 1999). Monthly flat-field data exists for filters F110W and F160W in camera 1; F110W, F160W and F222M in cameras 2 and 3. Only a few data sets were available for each of the remaining filters for the given period. Tables A.1, A.2 and A.3 in the appendix detail the full sampling of flat-field images used in this analysis.

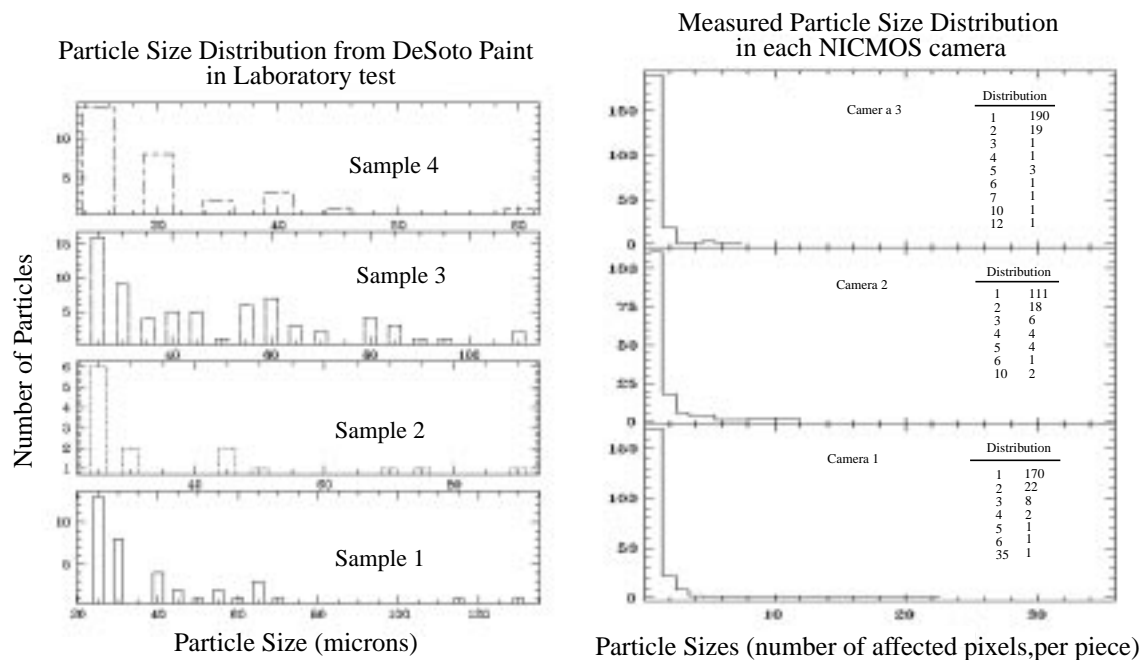


**Figure 3:** The plot on the left illustrates the results of the scrape test which examined the possible size distribution of the grot in a lab setting. The graphs on the right show the measured size distribution in all three NICMOS cameras. Note: it is not possible to determine the size distribution of pieces which may be smaller than one pixel, however the distribution in each of the cameras suggests that the majority of the grot affects single pixels.

Several different methods were investigated for beating down the background noise in order to pick out the grot. The final process involved recalibration of the lamp-on and lamp-off images through the NICMOS pipeline, similar to the method described by Schultz et al (NICMOS-ISR-98-003) for making reference flats. However, no more than 12 images were combined to make any one flat, so the S/N is lower than the recommended reference files. The image headers were updated, setting the calibration switches **FLAT-CORR=OMIT**, since we are working with flat-fields, **UNITCORR=PERFORM**, which converts units to count rates (DN/sec) by dividing the science and error images by the **SAMPTIME** keyword. The headers were also updated to reflect the most current linearity file and the appropriate synthetic dark file. The raw images were then run through **CALNICA**.

Since NICMOS does not have a shutter, lamp-off sky images are taken in order to sample the background. Lamp-on and lamp-off images were combined using **MSCOMBINE** and the resulting images subtracted from each other. The exception to this were flats taken before July 1997. The majority of these did not have corresponding lamp-off images so they were merely medianed together to form the combined image.

The new images were then normalized by the mean, inverted and ratioed with the appropriate ground flat. The resulting image was then run through a ring median filter (using the **RMEDIAN** task in IRAF), using an annulus 2 pixels wide with an inner radius of 3 pixels. This is essentially a low-pass filter which identified large variations within the image brought about by the temperature difference between the ground and inflight flat. The result was subtracted from the original ratioed image. This left an extremely flat image where grot and bad pixels dominate the statistics. A typical example of the end-product of this procedure can be seen in Figure 4. The line plot from a fully processed image clearly shows the two pieces of grot.

Image statistics were computed using **IMSTAT** for the image areas [1:256,36:256] in cameras 1 and 2 and [1:256,56:256] in camera 3, avoiding vignetted regions in the respective cameras. Grot is identified through iterative clipping above and below the mean in the final image. The final clipping values for each camera were all 3 sigma above the mean value in the respective images. Some of the grot pieces have bright edges, clipping above the mean allows these to be detected, although this only accounts for a few affected pixels in each camera.

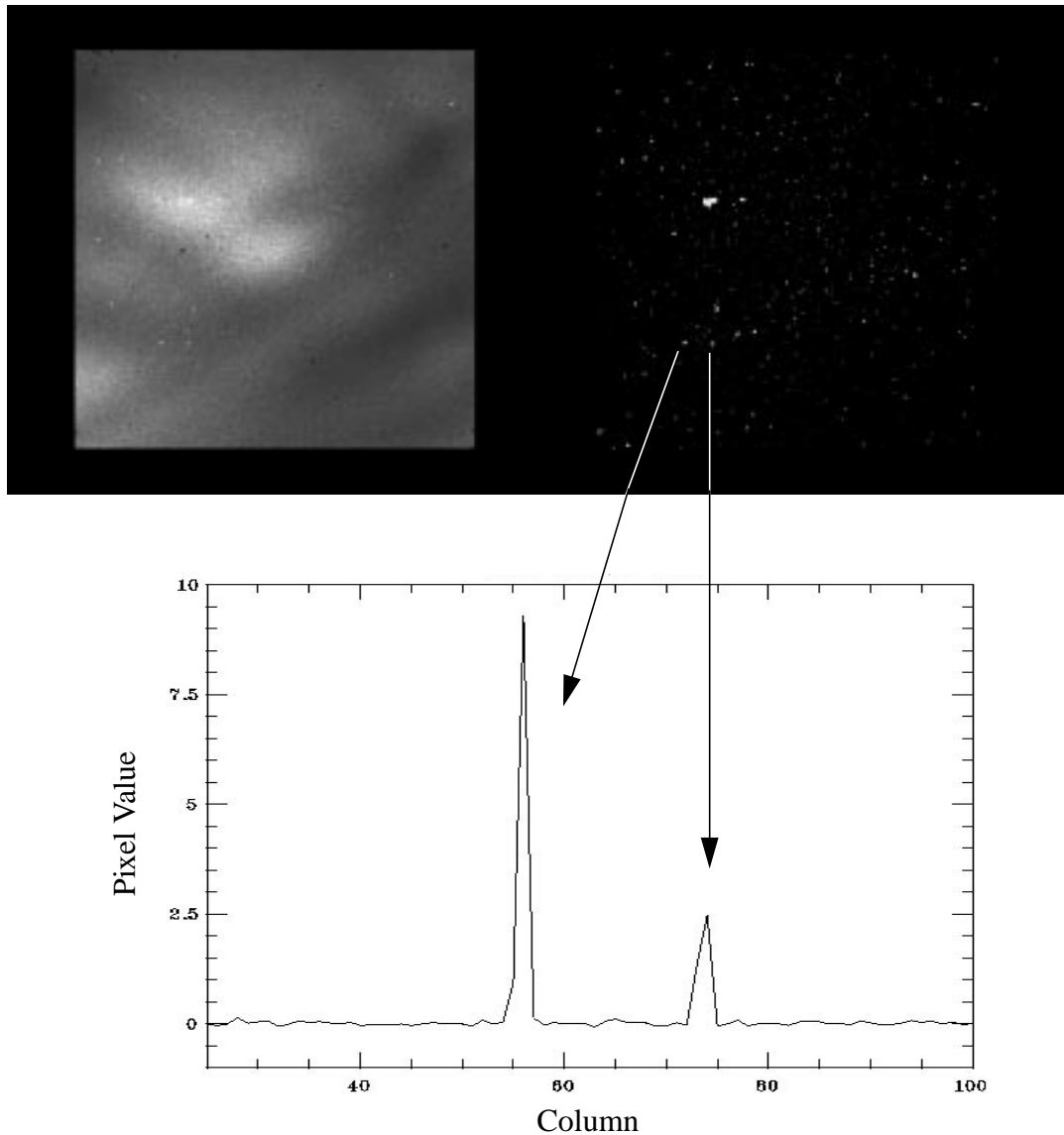


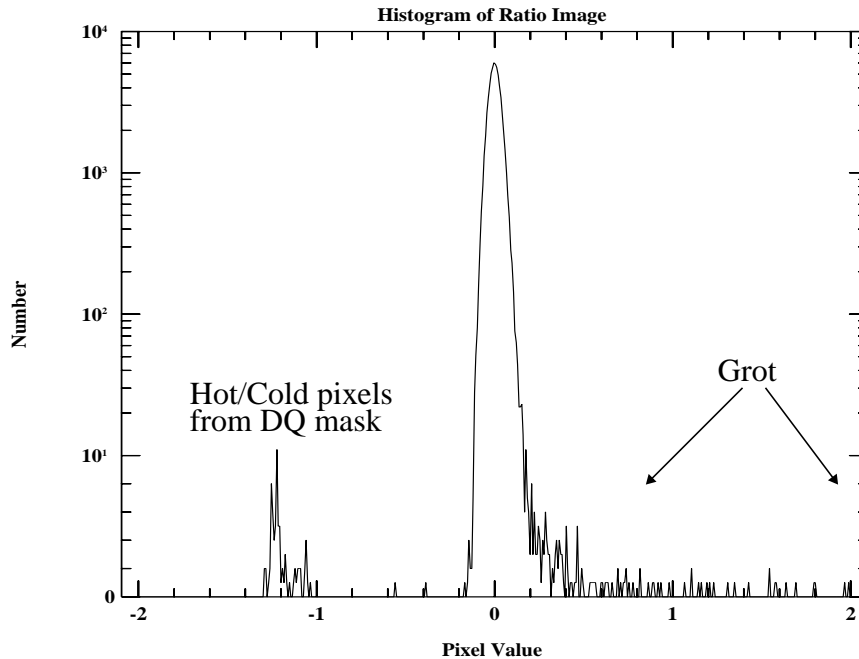
**Figure 4:** Two intermediate images in the grot finding process from camera 1. The image on the upper left is the combined lampOn - lampOff image. The upper right image is the fully processed image from which the clipping is done. It is stretched so that the grot (white pieces) are most easily seen. Above is a line plot showing the signature of 2 different pieces of grot.

There appears to be an underlying, consistent population of pixels which vary in sensitivity on a time scale of less than one month. Comparison of daily images taken during end of life (EOL) activities shows that it is possible for them to vary even on a daily basis. These pixels should not be grouped with the grot because they generally have a higher sensitivity. As a simple check, individual imsets of a lamp-on multiaccum image

were ratioed. Since the pixels in question did not stand out in the ratio images, they were not included in the grot masks.

Figure 5 shows the “dirty” histogram of a camera 1, F110W image, which is typical of all the cameras and filters. “Dirty” refers to the fact that grot, bad pixels, and the coronagraphic hole, in the case of camera 2, have not yet been corrected for and still have a large effect on the image statistics. Figure 5 also shows the difference between grot, which is present to the right of the image histogram, previously known hot/cold pixels, which cluster to the far left (remember that the image has been inverted, so most of the grot shows up above the mean). Previously known hot and cold pixels from ground testing are zeroed in the calibration process, and hence end up with highly negative values after the above processing is completed. New cold pixels are somewhat harder to detect, since they have characteristics much like the grot in the flat-fields, as such there may be new cold pixels present in the grot masks. The known bad pixels, all of which were determined from ground testing, are included in the DQ image and are subtracted from the grot masks in the final step of processing.

**Figure 5:** Histogram of a NIC1 F110W processed image



Detection at all thresholds reveals no wavelength dependence. Grot position in all the filters does not change to any great extent over the examined time scale, and the amount of grot since December 1997 has remained constant.

**Table 1.** NICMOS Cosmetics

Type	NIC1	NIC2	NIC3
Hot Pixels	10	11	3
Cold Pixels	68	94	17
Pixels affected by Grot	284	227	288

### 3. Results and Conclusions

Flat-field monitoring programs were active through January 6, 1999 when NICMOS' mean temperature reached 78.1 K, the limit of the mounting cup temperature sensors. Flat-fields taken between February 1997 and January 1999 were examined and the resulting images show no significant changes in the grot, hot or cold pixels after December 1997. New analysis should be performed on the flat-fields during SMOV3b, after the NCS is installed and NICMOS is cooled down to its new operating temperature. Observations should be obtained to investigate any further changes in the grot and detector cosmetics.

Dithering observations is the best way to guard against grot. Masks are necessary to remove the effect of grot in science images and provide a road-map for pixels about which one should be wary. Grot masks will be made available for each of the cameras on the NICMOS instrument website and should be used to correct data taken between July 1997 and November 1998. The masks are made up of simple 1's and 0's, 1 indicating a pixel affected by grot. They may be used with IRAF tasks such as **FIXPIX** which will replace the specified bad pixels though interpolation, or as part of the bad pixel masking in the Drizzle package (A.S. Fruchter and R.N. Hook). Figure 6 shows example grot masks for each of the cameras.

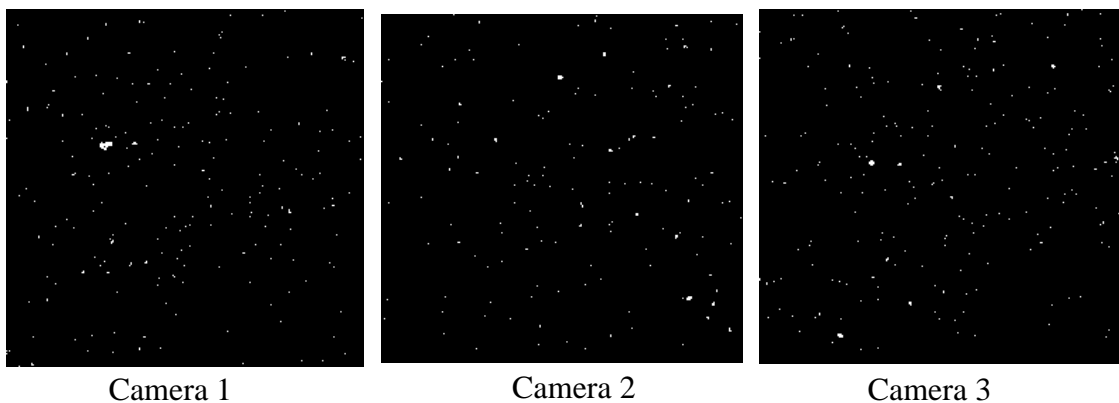


**Figure 6:** NIC1, NIC2 and NIC3 grot masks

## 4. Appendix

**Table A.1.** Flat-field coverage for NIC1

NIC 1		
Filter	Program ID	Dates Available
F090M	7775	7/97, 8/98
F095N	7041,7042 7043,7134 7608,7956	3/97-8/97 5/98
F097N	7042,7689 7956	3/97,2/98,5/98
F108N	7042,7956	3/97, 5/98
F110M	7690 & 7957	7/97 - 10/97, 8/98
F110W	7134,7690 8083,7957 7961	3/97, 8/97 - 1/99
F113N	7956	5/98
F140W	7957 & 7690	8/97, 8/98, 9/98
F145M	7690 & 7957	8/97, 8/98
F160W	7690,7957 7961,8083	7/97 - 1/99
F165M	7957 & 7690	8/97, 8/98
F166N	7111,7689 7956	4/97, 2/98, 5/98
F170M	7690 & 7957	8/97, 8/98
F187N	7111, 7689 7956	4/97, 2/98, 5/98
F190N	7111, 7689 7956	4/97, 2/98, 5/98
POL0S	7957 & 7690	7/97, 8/98
POL120S	7957 & 7690	7/97, 8/98
POL240S	7957 & 7690	7/97, 8/98
F164N	7111,7689 7956	4/97, 2/98, 5/98

**Table A.2.** Flat Field Coverage for NIC2

NIC 2		
Filter	Program ID	Dates Available
F110W	7041,7043,7046 7053,7134,7690 8083,7957,7961 7956,7150,7608 7042	3/97 - 1/99
F160W	7690,8083,7957 7961,7956	8/97 - 1/99
F165M	7690,7957,7956	8/97, 5/98
F171M	7042,7956,7690	3/97, 7/97, 5/98
F180M	7042,7956,7690	3/97, 8/97, 5/98
F187N	7956 & 7690	8/97, 5/98
F190N	7956 & 7689	2/98, 5/98
F204M	7957,7956,7690	8/97, 5/98, 8/98
F205W	7690,7956,7957	8/97, 5/98, 8/98
F207M	7956 & 7957	5/98, 8/98
F212N	7111,7956,7689	4/97, 2/98, 5/98
F215N	7111,7956,7689	4/97, 2/98, 5/98
F216N	7956 & 7689	2/98, 5/98
F222M	7690,7957 7956	7/97 - 1/99
F237M	7690,7956,7957	8/98, 5/98, 8/98
POL0S	7690 & 7957	7/97, 8/98
POL120S	7690 & 7957	7/97, 8/98
POL240S	7690 & 7957	7/97, 8/98

**Table A.3.** Flat-field coverage for NIC3

NIC3		
Filter	Proposal ID	Dates Available
F108N	7041,7042,7814 7134,7150,7608	3/97,4/97,12/97 6/97,7/97
F110W	7690,7957 8083,7814 7961,7046	3/97-5/97 8/97 - 1/99
F113N	7042 & 7814	3/97, 12/97
F150W	7814	12/97, 1/98
F160W	7690,7957 8083,7814 7961,7053	4/97, 8/97 - 1/99
F164N	7042 & 7814	3/97, 12/97
F166N	7814	12/97
F187N	7814	12/97
F190N	7814	12/97
F196N	7814	12/97
F200N	7814	12/97, 1/98
F212N	7814	12/97
F215N	7814	12/97
F222M	7814,7690 8083,7961 7957,7053	4/97 11/97 - 1/99
F240M	7814	12/97